NATIONAL ADVISORY COMMITTEE FOR AERONAUTICS

TECHNICAL NOTE 4221

TURBULENT FLOW THROUGH POROUS RESISTANCES SLIGHTLY INCLINED TO THE FLOW DIRECTION

By Albert L. Loeffler, Jr. and Morris Perlmutter

Lewis Flight Propulsion Laboratory
Cleveland, Ohio

Washington
February 1958

NATIONAL ADVISORY COMMITTEE FOR AERONAUTICS

TECHNICAL NOTE 4221

TURBULENT FLOW THROUGH POROUS RESISTANCES SLIGHTLY INCLINED TO THE FLOW DIRECTION

By Albert L. Loeffler, Jr. and Morris Perlmutter

SUMMARY

Analytical and experimental studies have been made of the channel flow of air through porous resistances inclined at an angle of $3\frac{1}{2}^{\circ}$ to the axis of the channel with the air discharging to the atmosphere. These studies determine the channel wall shape that would yield a uniform discharge through the porous resistance.

INTRODUCTION

Although flow through a resistance inclined to the flow direction is not a new concept, the number of applications of this type of flow has increased rapidly in recent years. For instance, heat exchangers employing oblique flow can be built more compactly and present much less frontal area than perpendicular-type heat exchangers. Oblique-flow air dryers have been used for similar reasons. Side air intakes for coolers on aircraft and various types of intake manifolds are other important examples of applications of oblique flow. Since the pressure drop through a porous resistance in turbulent flow varies approximately as the square of the normal velocity (refs. 1 to 3), it is seen that in theory the pressure drop will be less in oblique flow than in perpendicular flow for the same total flow rate and the same frontal area.

Though it appears that oblique flow possesses many inherent advantages, important difficulties exist in practice. First, because the fluid entering the porous resistance transfers a portion of its original momentum to the fluid remaining in the channel, there is a strong tendency for a nonuniform pressure to develop along the screen (refs. 4 and 5). This in turn results in nonuniform discharge through the resistance, which can be highly undesirable for applications such as heat exchangers where the over-all heat transfer would be decreased and hot spots could develop. The second difficulty is the turning loss experienced by the fluid as it

changes its direction to enter the porous resistance (refs. 6 and 7). This loss can be quite high in the case of large incoming velocities.

One method employed in the past to overcome these difficulties is the use of turning vanes (ref. 6), which, in general, are difficult to fabricate and install and do not always remove the difficulties. Another method of treating the previously mentioned difficulty of nonuniform pressure distribution along the porous resistance is to shape correctly the wall of the channel containing the resistance. In order to predict theoretically the wall shape which will give constant pressure along the resistance and hence uniform discharge through the resistance, it is necessary to know the fraction of momentum transferred by the fluid entering the resistance to the fluid left in the channel. This fraction is denoted by the symbol β.

Several theoretical studies have been made of channel wall shape, with various restricting assumptions on β. Thus, Keller (ref. 8) and Van Der Hegge Zijnen (ref. 9) have considered shaping the walls in manifold flow, assuming $\beta = 0$, and have found that the cross-sectional area of the channel must decrease linearly to zero. Cichelli and Boucher (ref. 4) assumed $\beta = 1$ in obtaining pressure distributions for different assumed wall shapes in connection with the problem of designing the headers on heat exchangers to give uniform flow through the pipes. Küchemann and Weber (ref. 7) have made a study of the optimum contours of airplane air intake walls, but their main purpose was to shape the walls so as to prevent separation and, hence, reduce pressure losses.

This report makes a more thorough experimental and analytical study of shaping the channel wall in order to obtain uniform discharge through the porous resistance by making the static pressure constant inside the channel. The analysis is made leaving the value of β undetermined, and the experiment is made in order to determine the value of β and the validity of the analysis. The particular configuration and flow conditions studied are those which will give a large tendency to nonuniform flow through the resistance: a small angle of inclination $\left(3\frac{1}{2}^\circ\right)$ of the porous resistance to the channel axis and a large incoming velocity head (of the same order of magnitude as the pressure drop through the porous resistance).

SYMBOLS

g acceleration of gravity

h head

K constant in eq. (A1) describing normal flow through a porous resistance

L	length of porous resistance in x-direction
m	exponent in eq. (A1) describing normal flow through a porous resistance
P	total pressure
p	static pressure
Re	Reynolds number, $2ru/\nu$
r	height of channel
u	mean velocity in x-direction
v_n	normal mean velocity component of fluid passing through porous resistance
w	weight-flow rate
x	distance measured along porous resistance in axial direction from upstream end
β	fraction of the original x-momentum transferred to the fluid remaining in the channel by the fluid entering the porous resistance
ν	kinematic viscosity
ρ	density
τ_0	shear stress at wall

Subscripts:

i	properties at $x = 0$
max	maximum value
min	minimum value

EXPERIMENT

Apparatus

Dry air at 125 pounds per square inch gage was used. The air was filtered and was passed through a standard ASME orifice run and then through a control valve into an expansion chamber. The expansion chamber

was connected to the test section by a bellmouth in an attempt to obtain a uniform entering profile. The test section exhausted directly into the room.

The pressure drop across the orifice was read on a water manometer, and the static pressure upstream of the orifice was measured on a Bourdon gage.

The test section (fig. 1) consisted of a rectangular duct, one wall of which was a porous plate at an angle of $3\frac{1}{2}^{\circ}$ with the flow direction. One or more layers of cotton cloth could be placed on top of the porous plate to increase the flow resistance. Figure 2 shows photographs of the perforated plate and the cloth. Care was taken to avoid wrinkles in the cloth layers. In order to avoid bulging of the porous plate during an experimental run, reinforcing metal strips were set edgewise beneath the plate and along the length of the test section.

The upper wall, which was flexible, was made of 1/8-inch-thick Plexiglas. It could be raised or lowered at various points by bolts (see fig. 3) which were adjusted by hand. The entering height, 2 inches, compared to the width, 16 inches, was designed to approximate a two-dimensional model.

Instrumentation on the test section consisted of pressure taps located as shown in figure 1 along the centerline of the upper wall. The pressures were read on water manometers. The first tap, located before the flexible wall, was used in determining the over-all pressure drop.

In an earlier model of the oblique-flow apparatus which had a straight upper wall, it was possible to take velocity and static-pressure profiles by means of a static- and total-head probe which traversed from the upper wall to the porous plate. This probe could be positioned at any longitudinal station. Qualitative smoke studies were made in this apparatus by introducing smoke through a pitot tube.

A vane-type anemometer was available for rough-flow measurements of the air coming out through the porous resistance.

The inclined-resistance test section could be replaced by a test section having a resistance placed normal to the flow as shown in figure 4. Pressure drop and velocity data taken with this test section were needed to calculate the resistance coefficients of the porous resistance.

Passing air for a number of hours through a cloth resistance set in the normal-flow test section showed that there was no appreciable sediment in the airflow which could clog the cloth and increase its pressure drop. The normal-flow test section was also used to check the uniformity

of the cloth by means of pressure drop measurements on several samples of cloth. The resistance of the cloth was found to be constant.

Procedure

The first step in determining the wall shape which would yield a uniform discharge through the porous resistance was to adjust the airflow to the desired rate. Next, the screws (see fig. 3) along the sides of the flexible wall were adjusted until the manometers connecting the flexible wall pressure taps showed that the pressure was constant inside the channel. Since the pressure outside the resistance was also constant (atmospheric) and the cloth resistance was uniform, the flow of air through the resistance then had to be uniform, as was desired. Measurements of the wall shape were then made by means of a depth gage.

4744

ANALYSIS

In order to arrive at an upper wall shape which will result in uniform discharge through the porous wall, an analysis is performed which makes use of the one-dimensional incompressible momentum and continuity equations. The system and the control volume considered are shown in the following sketch. Actually, in the experimental work there was an angle of $3\frac{1}{2}^{\circ}$ between u_i and the x-direction. For the analysis, it is more convenient to assume them to be parallel, and the error is very small because of the small angle.

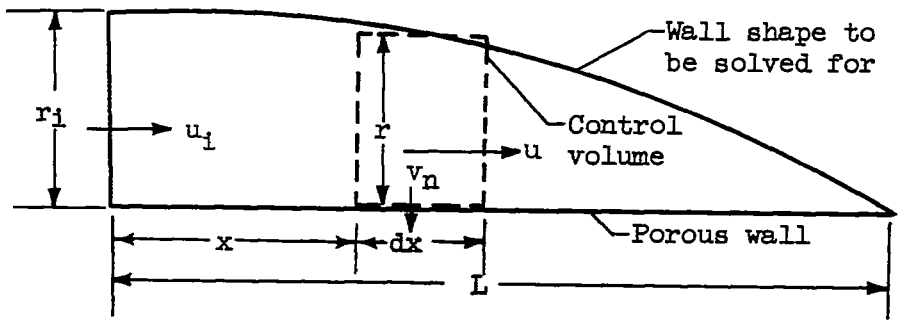

The conservation of momentum over the volume element gives

$$d(u^2r) + (1 - \beta)uv_n\,dx = -\frac{2\tau_0 g\,dx}{\rho} - \frac{rg\,dp}{\rho} \qquad (1a)$$

where β is the fraction of the x-momentum of the fluid leaving the bottom of the control volume that is transferred to the fluid left in the control volume and the continuity equation is

$$d(ur) + v_n\,dx = 0 \qquad (1b)$$

If v_n is eliminated from equation (1a) by means of equation (1b), the result is

$$d(u^2r) - (1 - \beta)u\, d(ur) = -\frac{2\tau_0 g\, dx}{\rho} - \frac{rg}{\rho}\, dp \tag{2}$$

In dimensionless form equations (2) and (1b) become, respectively,

$$d\left(\frac{u^2r}{u_i^2 r_i}\right) - (1 - \beta)\frac{u}{u_i}\, d\left(\frac{ur}{u_i r_i}\right) = -\frac{2\tau_0 g}{\rho u_i^2}\, d\left(\frac{x}{r_i}\right) - \frac{r}{r_i}\, d\left(\frac{pg}{\rho u_i^2}\right) \tag{3}$$

and

$$d\left(\frac{ur}{u_i r_i}\right) + \frac{v_n}{u_i}\, d\left(\frac{x}{r_i}\right) = 0 \tag{4}$$

Since the resistance of the porous wall is uniform, assuming constant pressure within the channel is the same as assuming a uniform discharge through the porous wall. Thus, the pressure term in equation (3) was set equal to zero, and v_n in equation (4) was taken as constant. Then equation (4) can be integrated to

$$\frac{u}{u_i} = \frac{1 - \dfrac{v_n x}{u_i r_i}}{\dfrac{r}{r_i}} \tag{5}$$

By over-all continuity, the flow entering the channel must be equal to that leaving through the porous wall, and, thus, for constant density:

$$v_n L = r_i u_i \tag{6}$$

Equation (5) may now be rewritten as

$$\frac{u}{u_i} = \frac{1 - \dfrac{x}{L}}{\dfrac{r}{r_i}} \tag{7}$$

The constant-pressure momentum equation is, by substitution of equation (7) into equation (3),

$$\beta\left(1-\frac{x}{L}\right)^2\frac{d\left(\frac{r}{r_i}\right)}{\left(\frac{r}{r_i}\right)^2}+(1+\beta)\left(1-\frac{x}{L}\right)\left[\frac{d\left(1-\frac{x}{L}\right)}{\frac{r}{r_i}}-\left(1-\frac{x}{L}\right)\frac{d\left(\frac{r}{r_i}\right)}{\left(\frac{r}{r_i}\right)^2}\right]$$

$$=2\frac{\tau_0 g}{\rho u_i^2}\frac{L}{r_i}\,d\left(1-\frac{x}{L}\right) \tag{8}$$

The Blasius resistance formula gives for the shear stress

$$\tau_0=0.0228\frac{\rho\nu^{1/4}u_{max}^{7/4}}{r^{1/4}} \tag{9a}$$

where u_{max} is the maximum velocity in the channel. The velocity u used in this analysis, however, is the mean velocity. If a 1/7-power turbulent velocity profile is assumed, $u_{max}=u/0.875$. If this expression for u_{max} is substituted into equation (9a), the result is

$$\tau_0=0.0288\frac{\rho\nu^{1/4}u^{7/4}}{r^{1/4}} \tag{9b}$$

It is now convenient to define a new variable y such that

$$y=1-\frac{x}{L} \tag{10}$$

If equations (9b) and (10) are substituted into equation (8), the result is

$$(1+\beta)y\,dy-y^2\frac{d\left(\frac{r}{r_i}\right)}{\frac{r}{r_i}}=0.0576\left(\frac{\nu}{r_i u_i}\right)^{1/4}g\frac{L}{r_i}\frac{y^{7/4}\,dy}{\frac{r}{r_i}}$$

This can be rewritten in the first-order linear form:

$$\frac{d\left(\frac{r}{r_i}\right)}{dy}-\frac{1+\beta}{y}\frac{r}{r_i}=-0.0576\left(\frac{\nu}{r_i u_i}\right)^{1/4}\frac{L}{r_i}\frac{1}{y^{1/4}} \tag{11}$$

assuming β is constant (see RESULTS AND DISCUSSION).

Then equation (11) integrates to

$$\frac{r}{r_i} = -0.0576 \left(\frac{\nu}{r_i u_i}\right)^{1/4} \frac{L}{r_i} \frac{y^{3/4}}{\beta + \frac{1}{4}} + Cy^{1+\beta} \tag{12}$$

At the beginning of the channel, $y = 1$, $r/r_i = 1$, and, therefore,

$$C = 1 - 0.0576 \left(\frac{\nu}{r_i u_i}\right)^{1/4} \frac{L}{r_i} \frac{1}{\beta + \frac{1}{4}}$$

Substituting this value of C into equation (12) and making use of equation (10) give

$$\frac{r}{r_i} = \left(1 - \frac{x}{L}\right)^{1+\beta} + \frac{0.0685}{\beta + \frac{1}{4}} \frac{L}{r_i} \frac{1}{(\mathrm{Re})_i^{1/4}} \left[\left(1 - \frac{x}{L}\right)^{3/4} - \left(1 - \frac{x}{L}\right)^{1+\beta}\right] \tag{13}$$

where

$$(\mathrm{Re})_i = \frac{2 r_i u_i}{\nu}$$

For given values of the parameters β, L/r_i, and $(\mathrm{Re})_i$, equation (13) gives the wall shape required to yield a uniform flow through the porous wall.

RESULTS AND DISCUSSION

Static-Pressure and Velocity-Head Profiles

Figure 5 shows representative static-pressure and velocity-head profiles obtained at various axial stations in the earlier model of the oblique-flow test section. The constancy of static pressure at a given cross section, as evidenced by figure 5(a), lends experimental support to the one-dimensional approach employed in the analysis. The velocity-head profiles of figure 5(b) show a boundary layer formed on the upper wall but indicate that the boundary layer has been appreciably reduced by suction through the screen on the other side.

Theoretical and Experimental Wall Shapes

Figure 6 shows the theoretical variation of the wall shape required for uniform pressure with the parameter β for the case of zero wall friction. Equation (13), with the friction term omitted, was used to obtain these curves. The curves vary from the parabola $r/r_i = (1 - x/L)^2$ for $\beta = 1$ to the straight line for $\beta = 0$. As shown next, the effect of friction is often small, so that the curves presented in figure 6 can often be used.

Figure 7 presents the curves obtained from equation (13) for four different values of Reynolds number and for a somewhat arbitrarily picked value of β of 0.2. The frictional effect becomes smaller with increasing Reynolds number. The larger channel height obtained when friction is considered is caused by the necessity of decelerating the flow to offset the frictional pressure drop.

The experimentally obtained "constant-pressure" wall shapes are compared with theoretical curves in figure 8. The theoretical curves are for values of 0, 0.2, and 0.4 for β and for an average value of 4×10^5 for $(Re)_i$. The approximate range of $(Re)_i$ in this investigation was from 2×10^5 to 6×10^5. The data for the perforated plate only as resistance follow most closely along the curve for $\beta = 0$, whereas the data for the plate-cloth combinations fall near the curve for $\beta = 0.2$. Irregularities in the curves near the upstream end may indicate an entrance effect. The reason for the plate-and-two-cloth combination data lying somewhat above those for the plate-and-one-cloth combination at the larger values of x/L is unknown.

During the experimental work the vane anemometer was used to confirm the fact that the constant-pressure wall shapes did result in uniform airflow through the resistance.

Apparently the problem of predicting the value of β from flow geometry and parameters is still unsolved. One of the most complete discussions of this subject appears in a paper by Soucek and Zelnick (ref. 5) in connection with manifold flow. These authors concluded from consideration of available manifold data that β was either a constant or a function of the ratio of the side tube flow to the main flow at a given point in the manifold.

McNown (ref. 5) claimed that β can never be more than 0.5. Comtois (ref. 6) concluded from smoke studies of oblique flow through screen matrices that all the turning takes place after the fluid has entered the matrix. For this situation a value of zero for β would be obtained. Thus, in general, the values of β found in the present report (0 to 0.2) are not contrary to information in the literature.

It would seem possible that a β of zero rather than 0.2 was obtained for the perforated plate because the larger openings of the plate allowed the fluid to enter the plate before turning. For the plate-cloth combinations, however, the openings were so small that the fluid was forced to turn before reaching them, thereby giving up 20 percent of its momentum to the fluid left in the channel.

Uncorrected and Corrected Pressure Distributions

Pressure distributions are shown in figure 9(a) for a straight upper wall for different flow rates in the representative case of the plate-cloth resistance. These curves show a rapid increase in pressure toward the downstream end of the channel. Physically speaking, the pressure rise is caused by the transfer of momentum from the fluid leaving through the resistance to the fluid left in the channel. The pressure oscillation near the start of the curves in figure 9(a) may be caused by an entrance effect.

Figure 9(b) is the same type plot as figure 9(a) but is for a shaped upper wall. The wall was shaped such that uniform pressure was obtained at an entrance velocity of 264 feet per second. The other pressure distributions were then obtained by maintaining the original wall shape and lowering the flow rate to various other values. Although the pressure distribution remains substantially uniform, there is a Reynolds number effect noticeable for the downstream tap where the pressure decreases for decreasing flow rate. The wall could be readjusted to give uniform pressure at the low flow rates, and, after this was done, the change in shape was so small that it would have been negligible if plotted on figure 8. This experimental finding can be justified by means of figure 7 which indicates only a small change in wall shape for such a small variation in $(Re)_1$.

Total-Pressure Drop Through Test Section

The data for total-pressure drop against flow rate for the perforated-plate, plate-and-one-cloth, and plate-and-two-cloth resistances are shown in figures 10(a), (b), and (c), respectively. In each case, data for both the straight upper wall and the shaped upper wall are included. The perforated plate (fig. 10(a)) shows almost no difference in total-pressure drop for the two wall shapes, which might be expected since the two wall shapes are almost identical. Figures 10(b) and (c), however, show that the wall shaped for constant pressure gives higher pressure drops than the straight upper wall in both cases. This is probably due to the fact that the adverse pressure gradient set up for the straight wall cases effects a higher turning efficiency.

The increase in total-pressure drop through the test section due to shaping the wall as a function of the nonuniformity of the uncorrected flow is shown in figure 11. The parameter of nonuniformity is taken as $v_{n,min}/v_{n,max}$ where $v_{n,min}$ is the minimum measured normal velocity and $v_{n,max}$ is the maximum measured normal velocity through the porous resistance. A value of 1 for the abscissa represents uniform flow, while smaller values represent nonuniform flow. The ordinate is the ratio of the total-pressure drop for uniform flow ΔP_{shaped} to the total-pressure drop for the uncorrected flow $\Delta P_{straight}$ for the same weight flow. The data plotted in figure 11 show that the greater the nonuniformity of the flow, the greater the total-pressure loss suffered in shaping the wall to make the flow uniform.

Also shown in figures 10(a) to (c) are the theoretical limiting curves of Küchemann and Weber (ref. 7). Their estimate I assumes 100-percent turning losses, and thus the pressure drop represented by this curve is equal to the sum of the straight-through pressure drop through the screen (see the appendix) and the entering velocity head parallel to the porous resistance. Their estimate II represents the case of minimum turning losses and depends upon whether the entering velocity head parallel to the resistance is less or greater than the straight-through pressure drop of the resistance. If it is less, then estimate II is just the straight-through pressure drop of the resistance. If it is greater, however, 100-percent turning efficiency would result in an over-all static-pressure increase across the resistance, a situation considered physically improbable. Therefore, estimate II in this case is equal to the entering velocity head parallel to the resistance.

It would be expected that the present data would fall between estimates I and II. For some reason, however, the data of figure 10(a) fall slightly above estimate I. The data of figures 10(b) and (c) are, as expected, between the two estimated curves. The preliminary smoke studies and velocity and pressure traverses indicated no great turbulence inside the channel and, therefore, it can be concluded that the greater part of the turning losses occurred not in the channel but inside the resistance.

SUMMARY OF RESULTS

Analytical and experimental studies were made of turbulent airflow through a porous resistance inclined at a small angle, $3\frac{1}{2}^{\circ}$, to the flow direction. The analytical studies were made assuming incompressible uniform flow with an unknown parameter β, defined as the fraction of the original momentum transferred to the fluid remaining in the channel by the fluid entering the porous resistance. The results of these studies are summarized as follows:

1. It is possible, by shaping the wall of an inclined-flow apparatus where the angle between the incoming flow and porous wall is small, to obtain uniform flow out of the porous wall.

2. The theory developed in this report can be successfully employed to predict the approximate wall shape needed to give uniform flow out of the porous wall if the value of β is known.

3. Values of β of 0 and 0.2 were obtained experimentally for the perforated plate and plate-cloth resistances, respectively, for the range of conditions studied.

4. Uniform flow through the porous wall is attained at the expense of increased loss of total pressure.

Lewis Flight Propulsion Laboratory
National Advisory Committee for Aeronautics
Cleveland, Ohio, December 11, 1957

APPENDIX - STRAIGHT-THROUGH POROUS RESISTANCE

It is customary to describe the pressure drop through a porous wall by an equation of the form

$$\Delta p = \frac{K\rho}{2g} v_n^m \tag{A1}$$

where v_n is the component of fluid velocity perpendicular to the wall and K and m are experimentally determined constants. For laminar flow the exponent m is equal to 1, while for turbulent flow it is approximately equal to 2. In terms of experimentally measured quantities equation (A1) can be written

$$5.2\ \Delta h = \frac{K\rho}{2g} (29.7\ w)^m \tag{A2}$$

Thus, the values of K and m for the three resistances used in this work were calculated from data for Δh plotted against w, obtained from the straight-through rig. The curves and calculated values are shown in figure 12. The K and m values were employed in computing the theoretical limiting lines of figure 10.

The values of the exponent m for the three curves were 1.90, 1.80, and 1.94. Therefore, the flow through the resistances can be assumed to be turbulent.

It is interesting to note from figure 12 that the effect of adding the second cloth (top curve) was not as great on the over-all resistance as that of the first cloth. Thus, the resistances are not simply additive as might be assumed.

More comprehensive treatments of the resistance of screens, cloths, and perforated plates placed perpendicular to the flow can be found in references 1, 2, and 3.

REFERENCES

1. Baines, W. D., and Peterson, E. G.: An Investigation of Flow Through Screens. Trans. ASME, vol. 73, no. 5, July 1951, pp. 467-477; discussion, pp. 477-480.

2. Hoerner, S. F.: Pressure Losses Across Screens and Grids. AF Tech. Rep. No. 6289, Wright Air Dev. Center, Wright-Patterson Air Force Base, Nov. 1950.

3. Hoerner, S. F.: Aerodynamic Properties of Screens and Fabrics. Jour. Textile Res., vol. 22, no. 4, Apr. 1952, pp. 274-280.

4. Cichelli, M. T., and Boucher, D. F.: Design of Heat-Exchanger Heads for Low Holdup. Preprint No. 58, Am. Inst. Chem. Eng., 1955.

5. Soucek, Edward, and Zelnick, E. W.: Lock Manifold Experiments. Trans. Am. Soc. Civil Eng., vol. 110, 1945, pp. 1357-1377; 1385-1400. (Discussion by John S. McNown, pp. 1378-1385.)

6. Comtois, W. H.: Oblique Flow Losses in Screen Matrix Heat Exchangers. Tech. Rep. 29, Dept. Mech. Eng., Stanford Univ., June 1956. (Contract N-onr-22523.)

7. Küchemann, Dietrich, and Weber, Johanna: Aerodynamics of Propulsion. Ch. 12. McGraw-Hill Book Co., Inc., 1953.

8. Keller, J. D.: The Manifold Problem. Jour. Appl. Mech., vol. 16, 1949, pp. 77-85.

9. Van Der Hegge Zijnen, B. G.: Flow Through Uniformly Tapped Pipes. Appl. Sci. Res., vol. A-3, 1951, pp. 144-162.

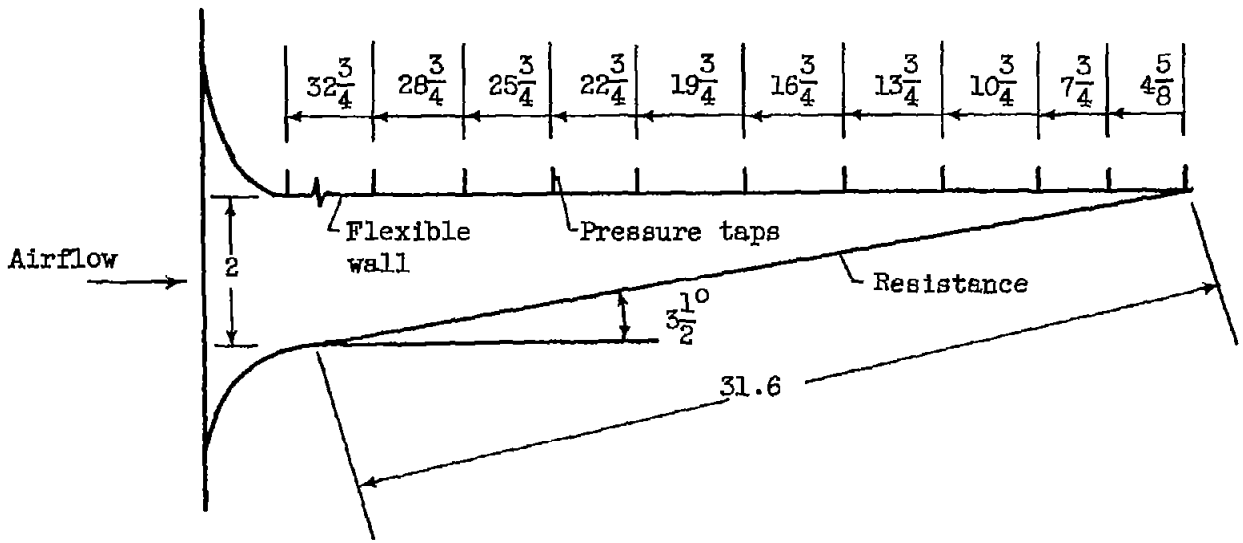

Figure 1. - Diagram of oblique test section. (All dimensions in inches except where noted.)

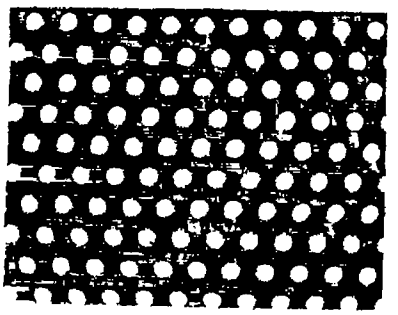

C-45857
Perforated plate, full size.

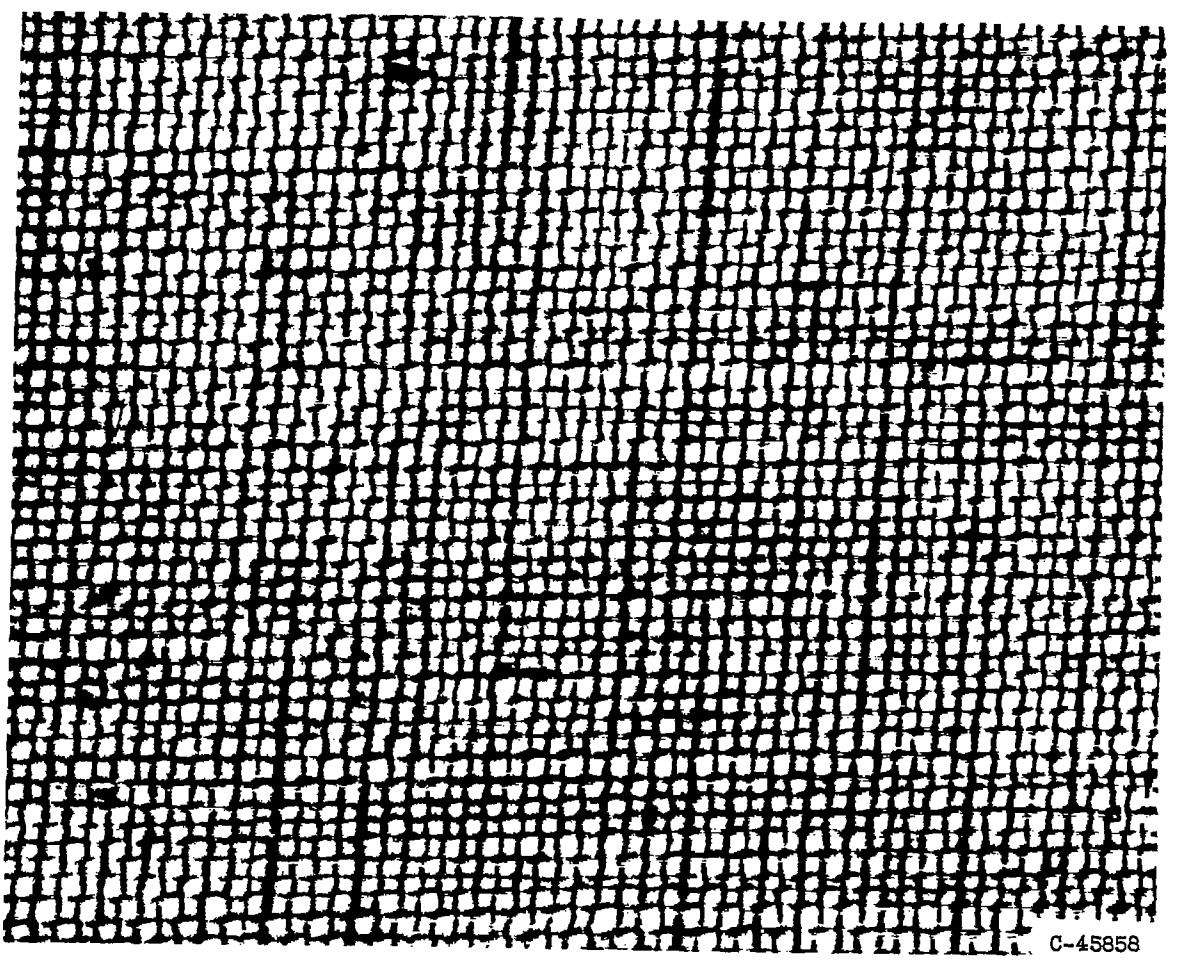

C-45858
Cloth, magnified 5 times.

Figure 2. - Perforated plate and cloth.

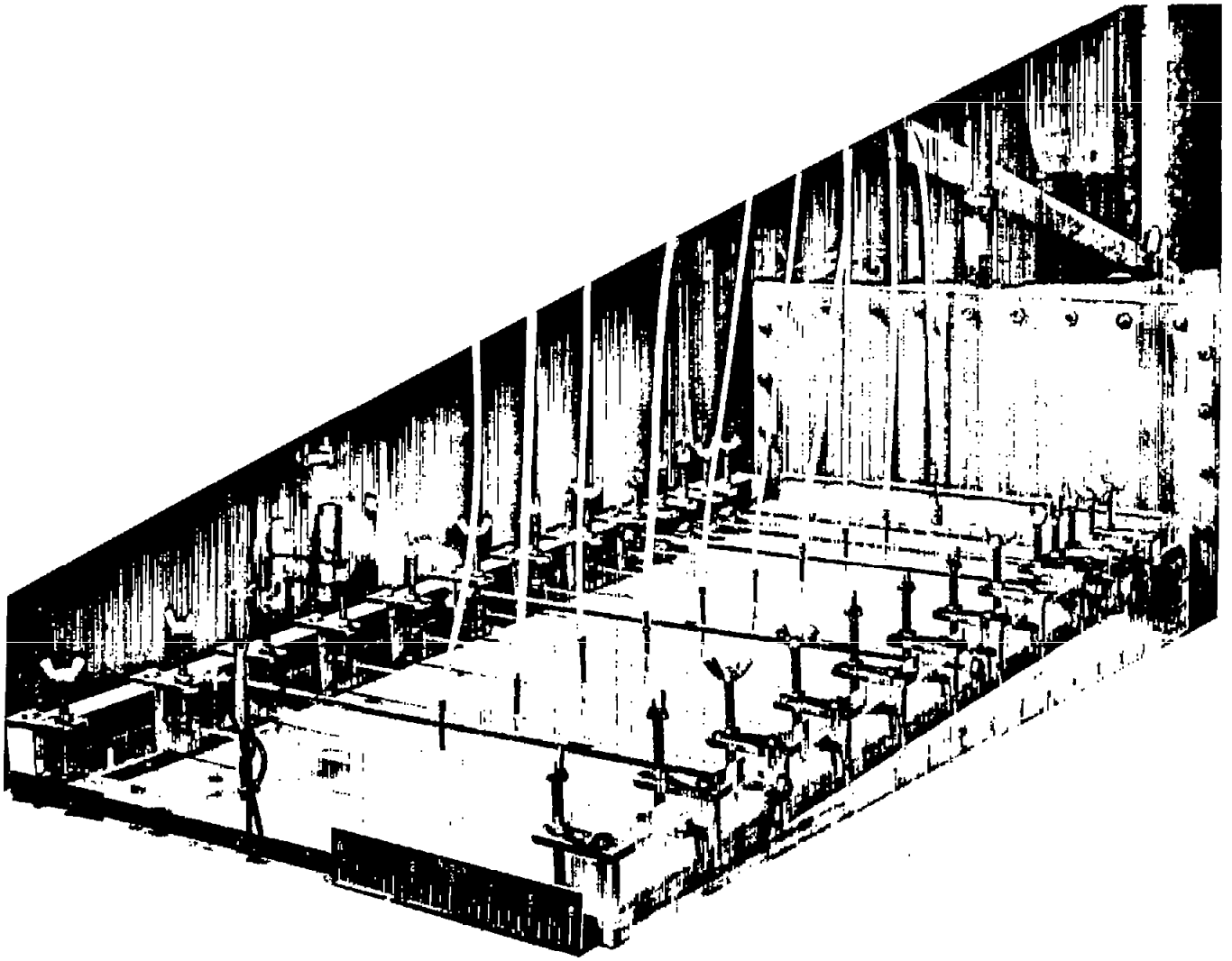

C-45856

Figure 3. - Over-all apparatus.

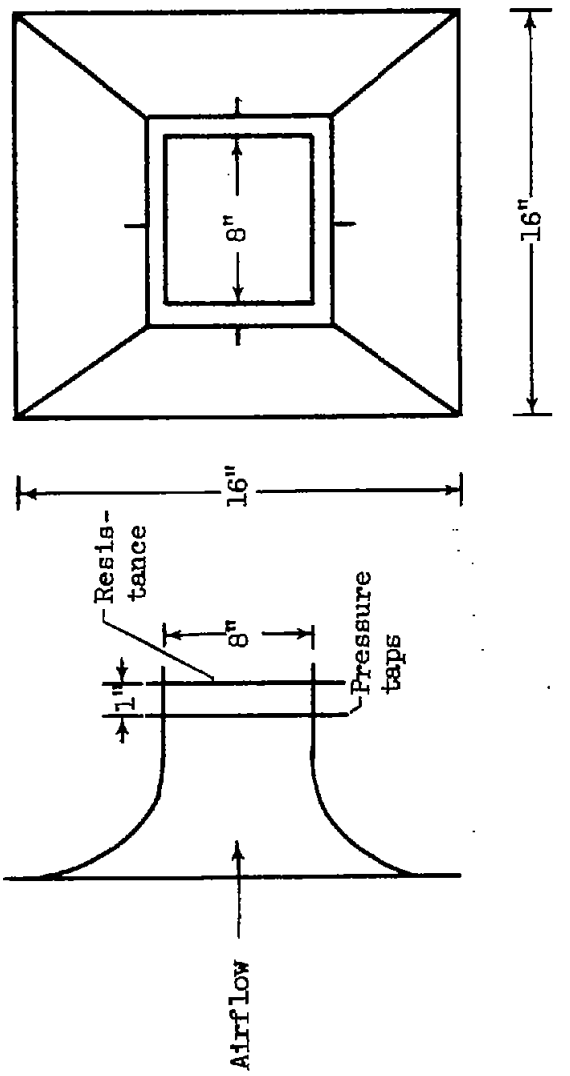

Figure 4. - Diagram of straight-through test section.

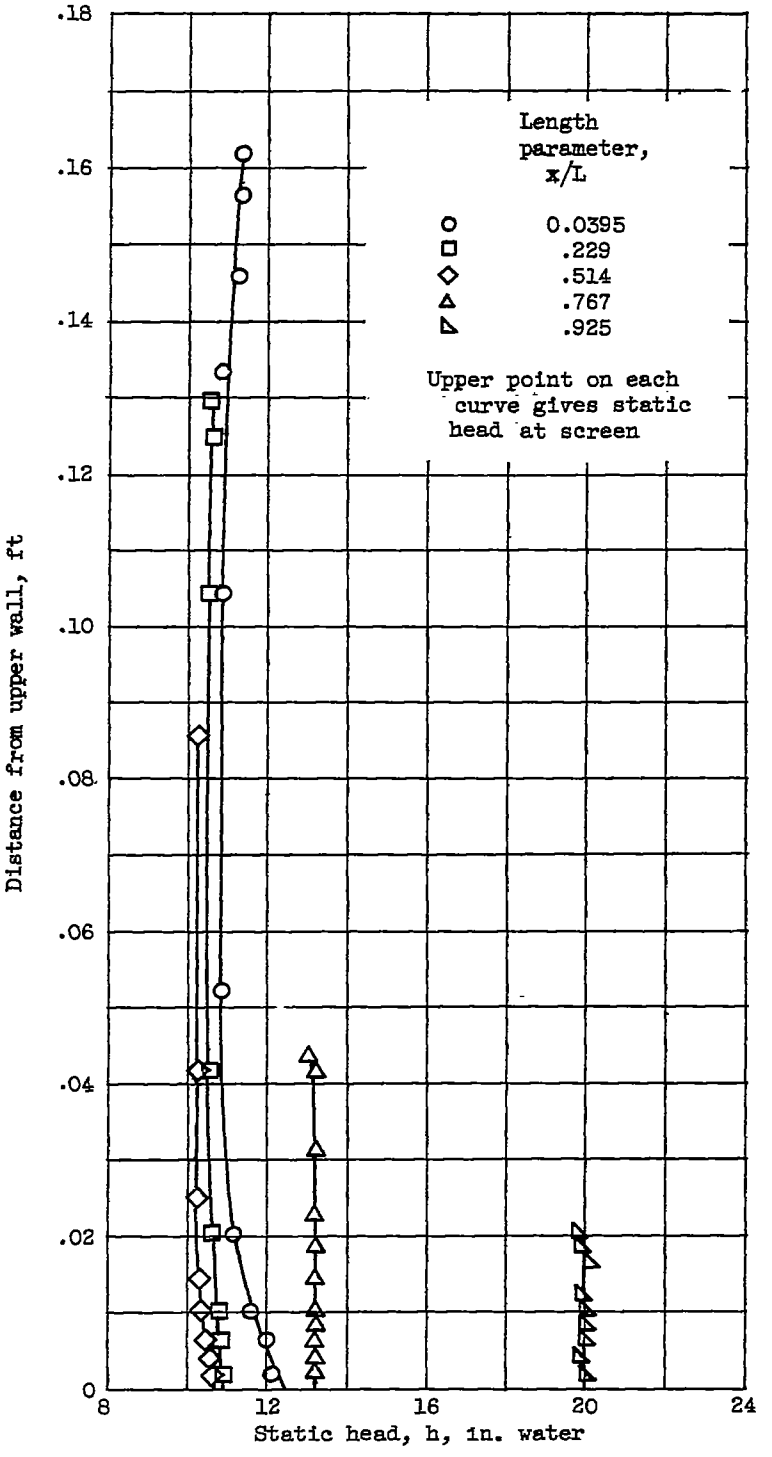

(a) Static head.

Figure 5. - Profiles obtained in earlier version of oblique-flow test section. $(Re)_1 = 4.17 \times 10^5$.

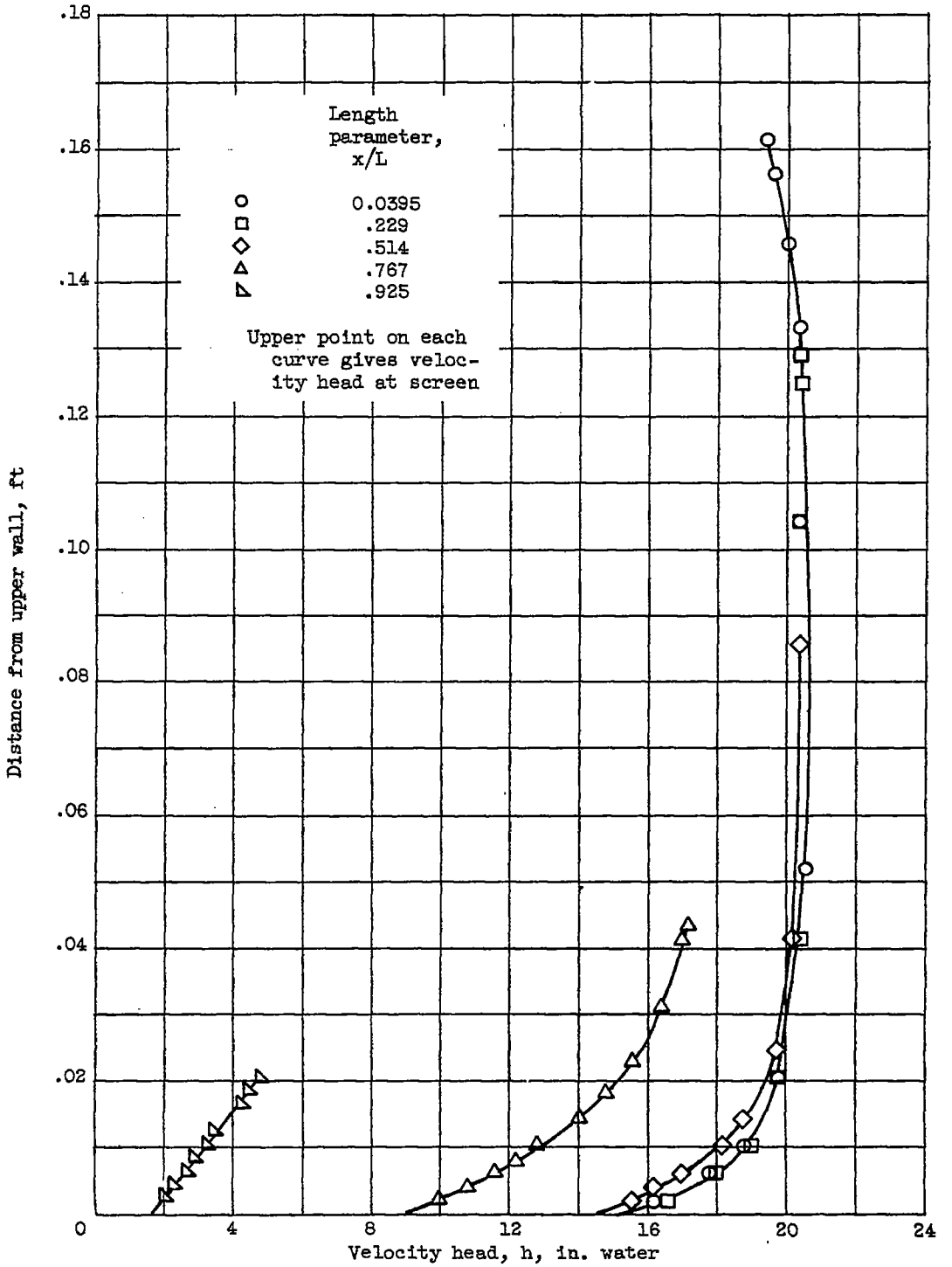

(b) Velocity head.

Figure 5. - Concluded. Profiles obtained in earlier version of oblique-flow test section. $(Re)_1 = 4.17 \times 10^5$.

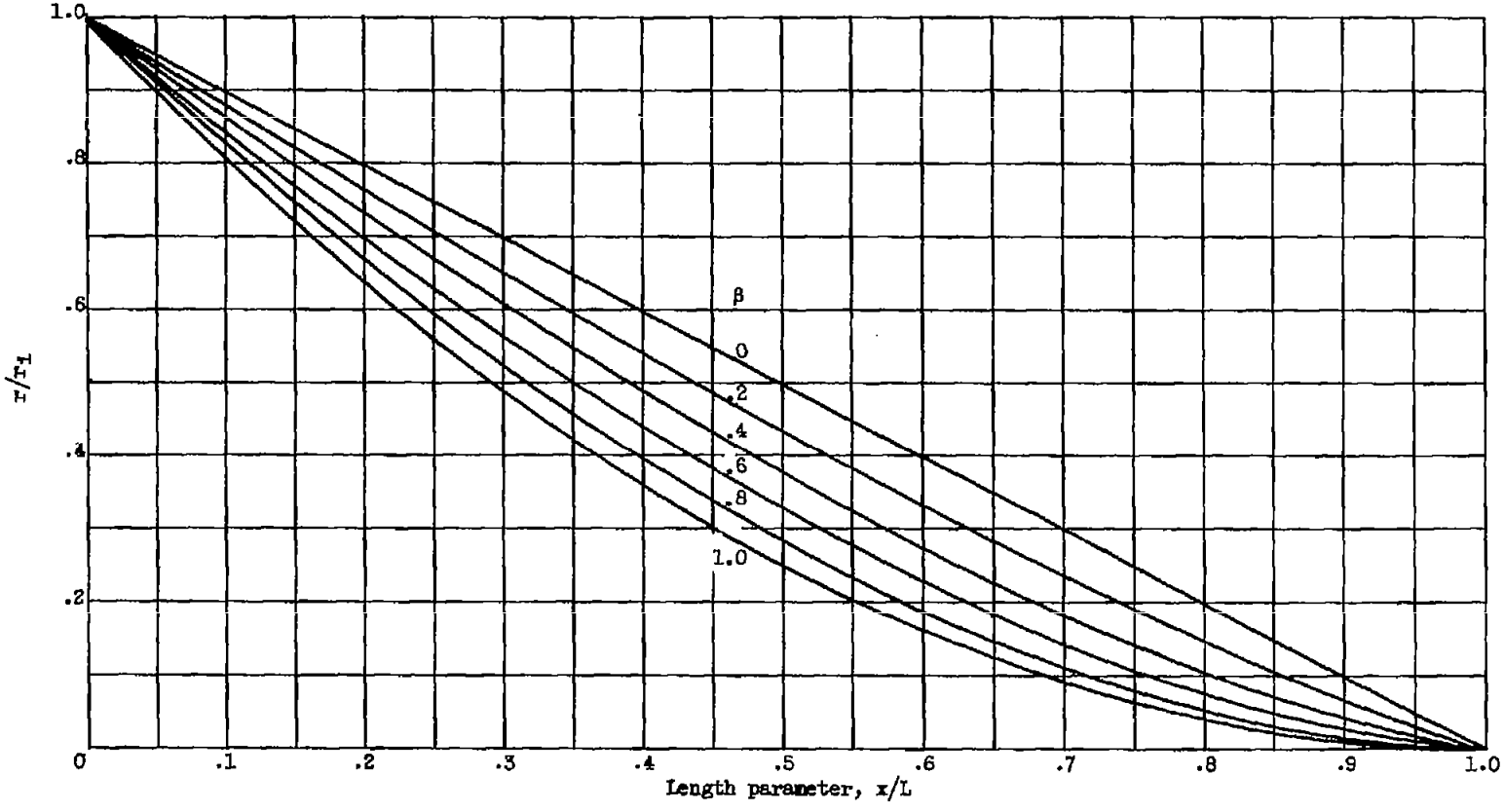

Figure 6. - Predicted variation of wall shape with β for zero wall friction.

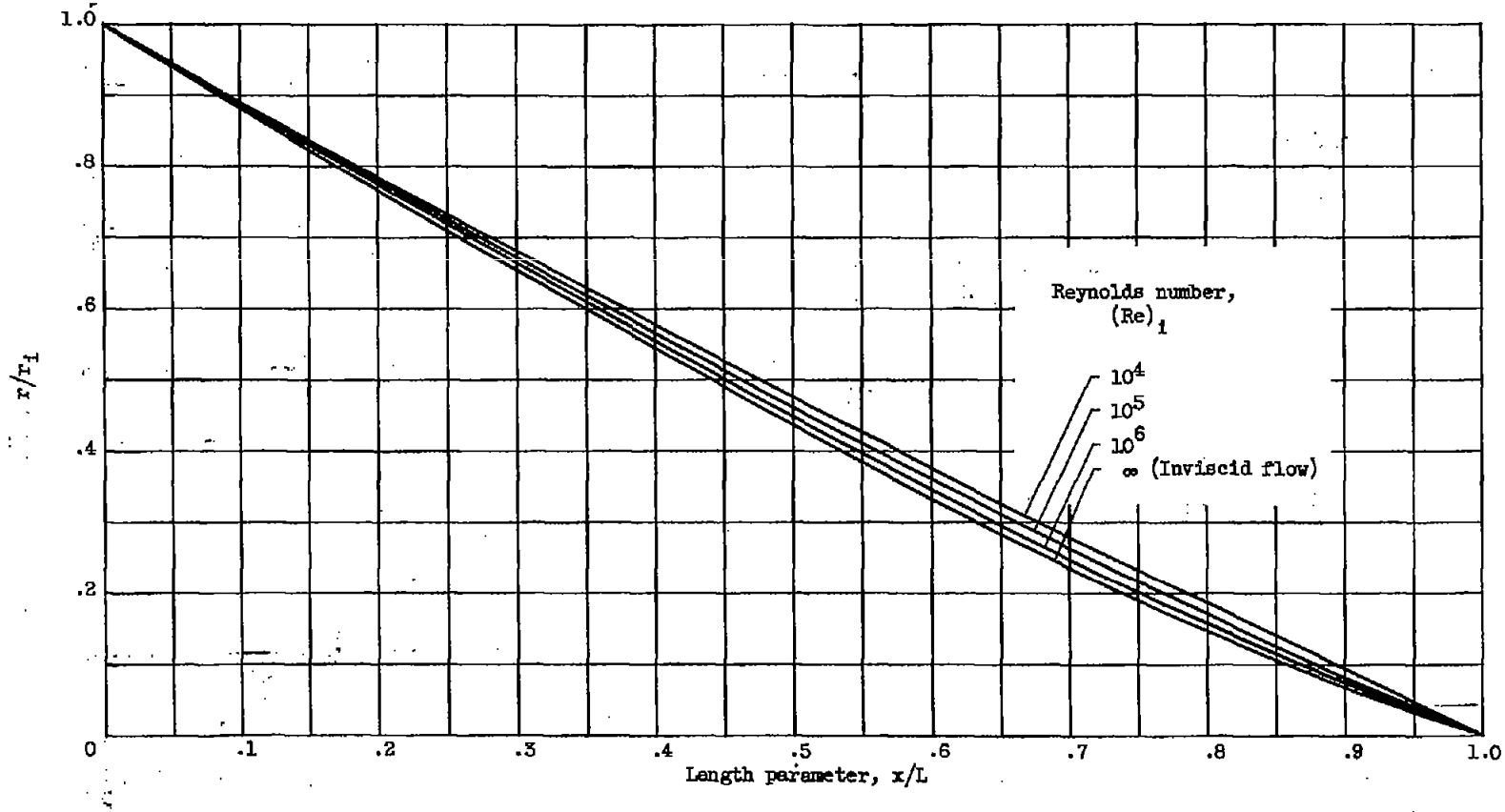

Figure 7. - Predicted Reynolds number effect on wall shape for $\beta = 0.2$.

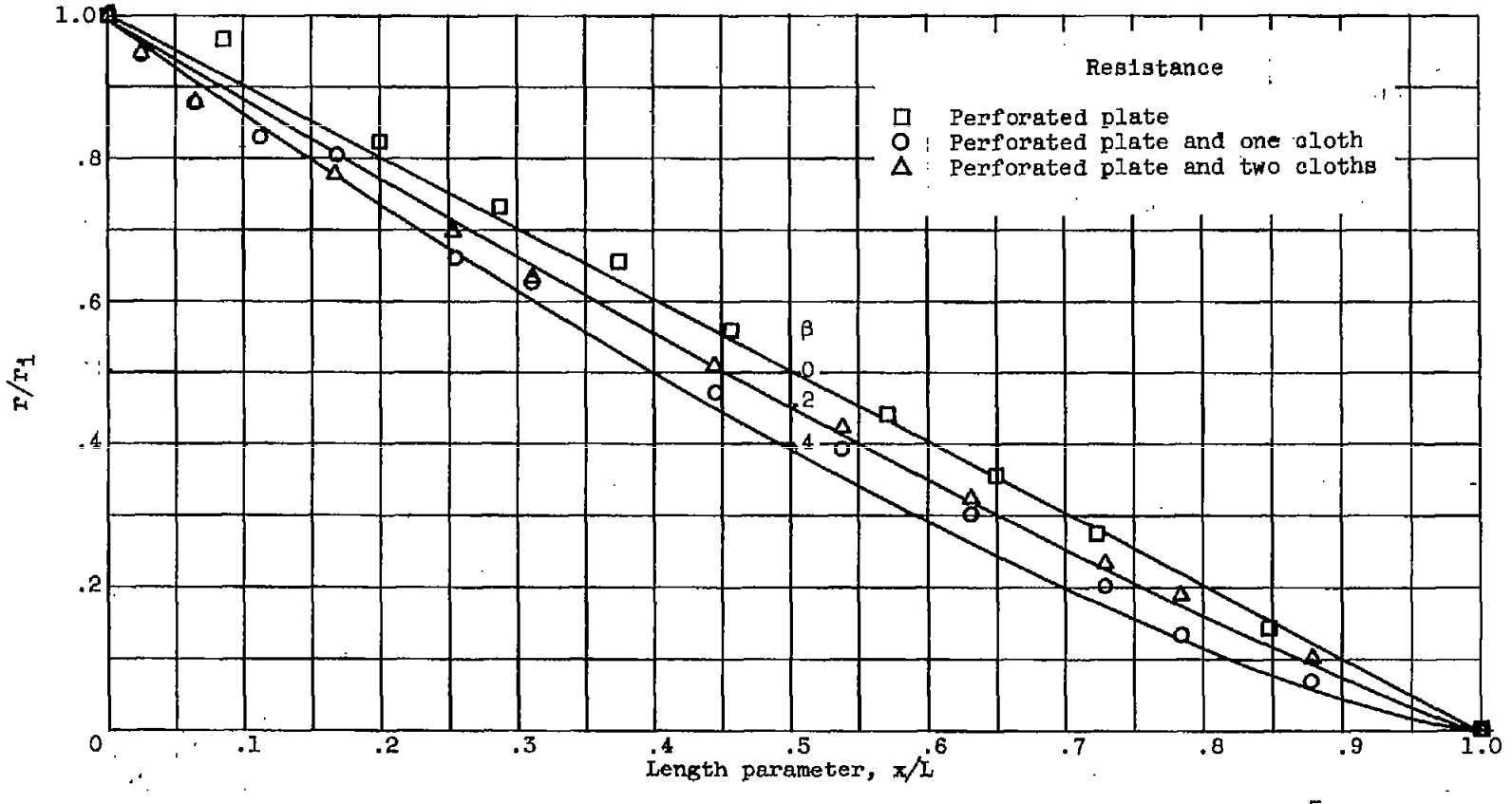

Figure 8. - Comparison of experimental wall shapes with theory. $(Re)_1 = 4 \times 10^5$.

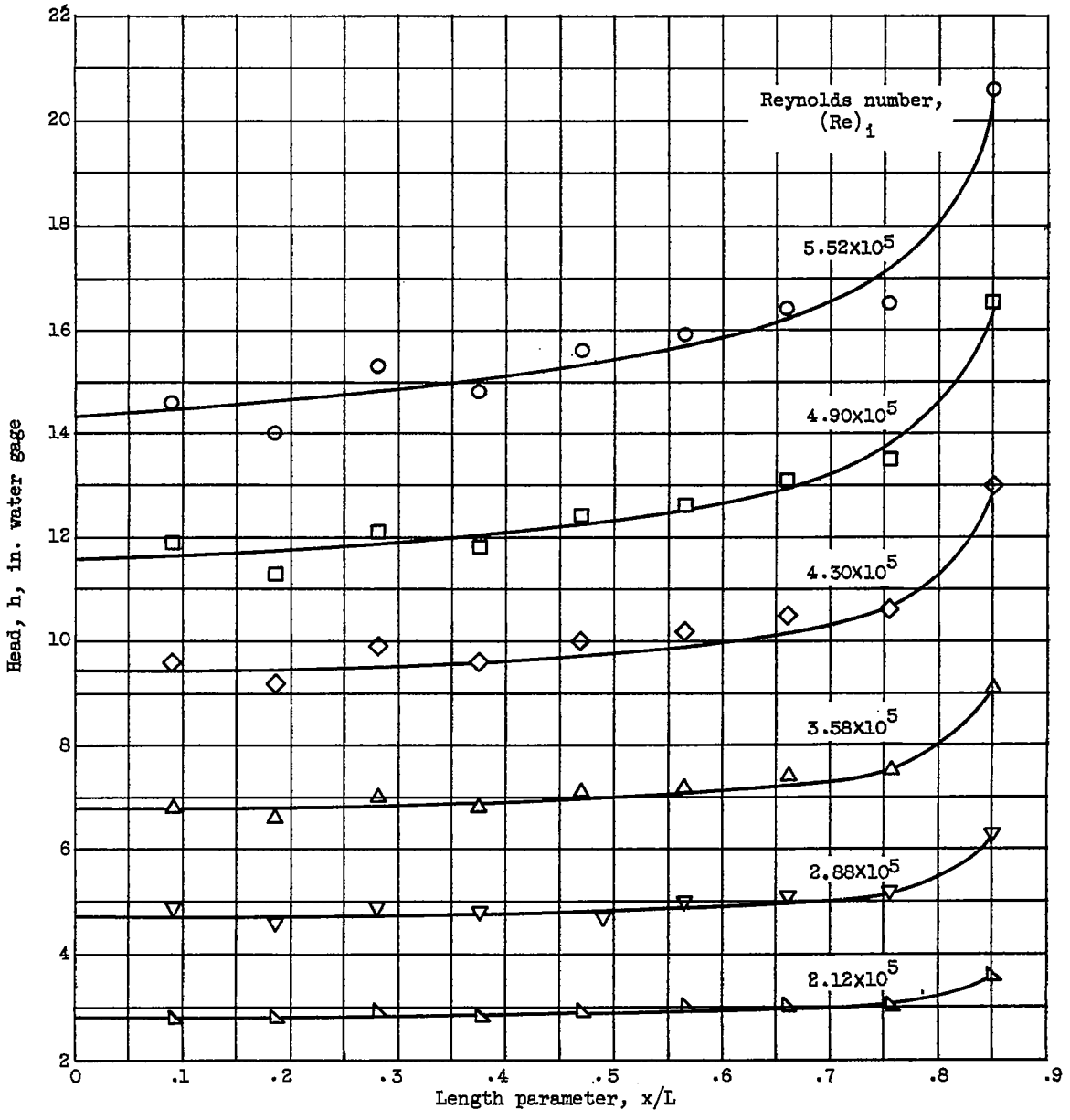

(a) Straight upper wall.

Figure 9. - Reynolds number effect on pressure distribution for various wall shapes using plate and one cloth.

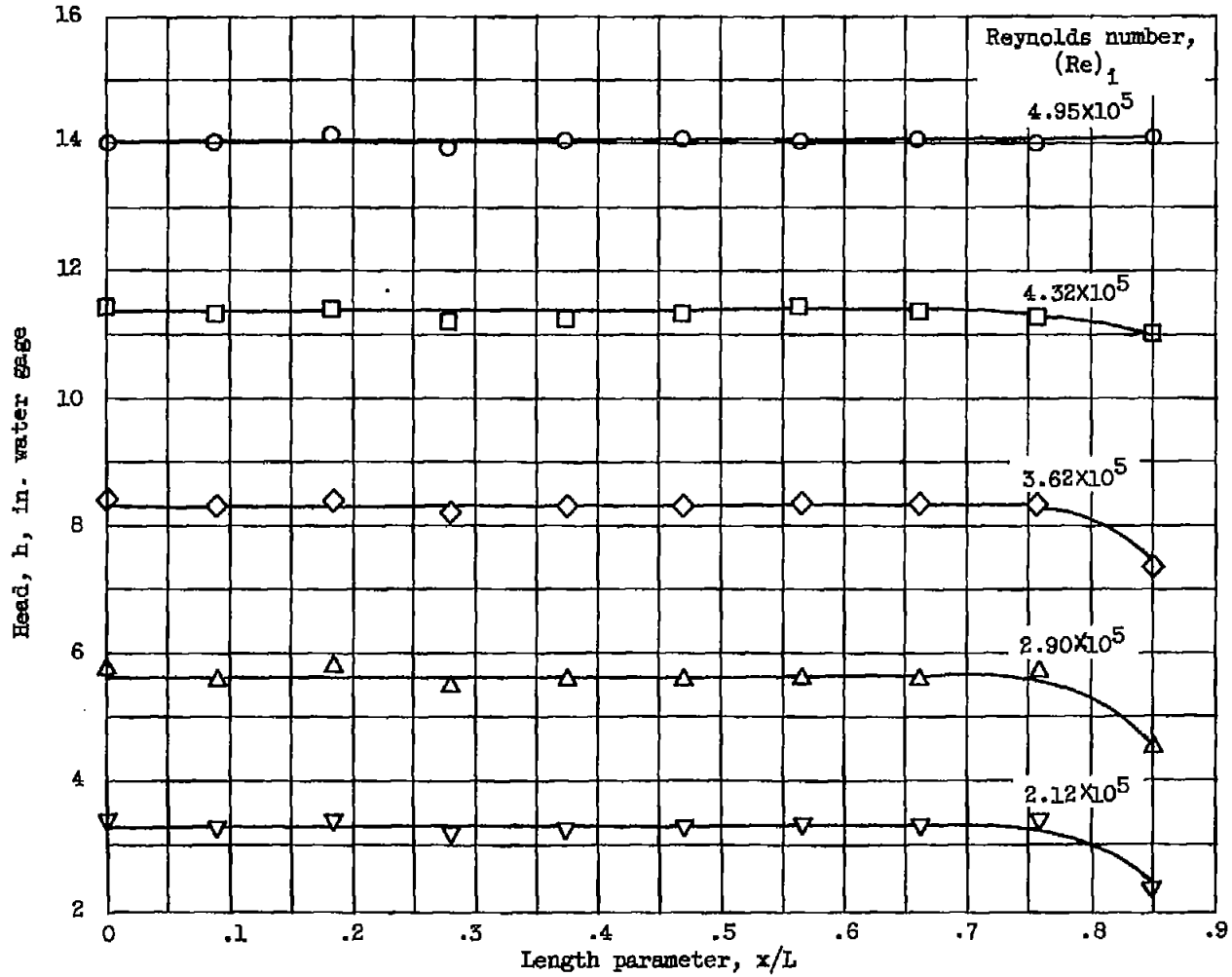

(b) Shaped upper wall.

Figure 9. - Concluded. Reynolds number effect on pressure distribution for various wall shapes using plate and one cloth.

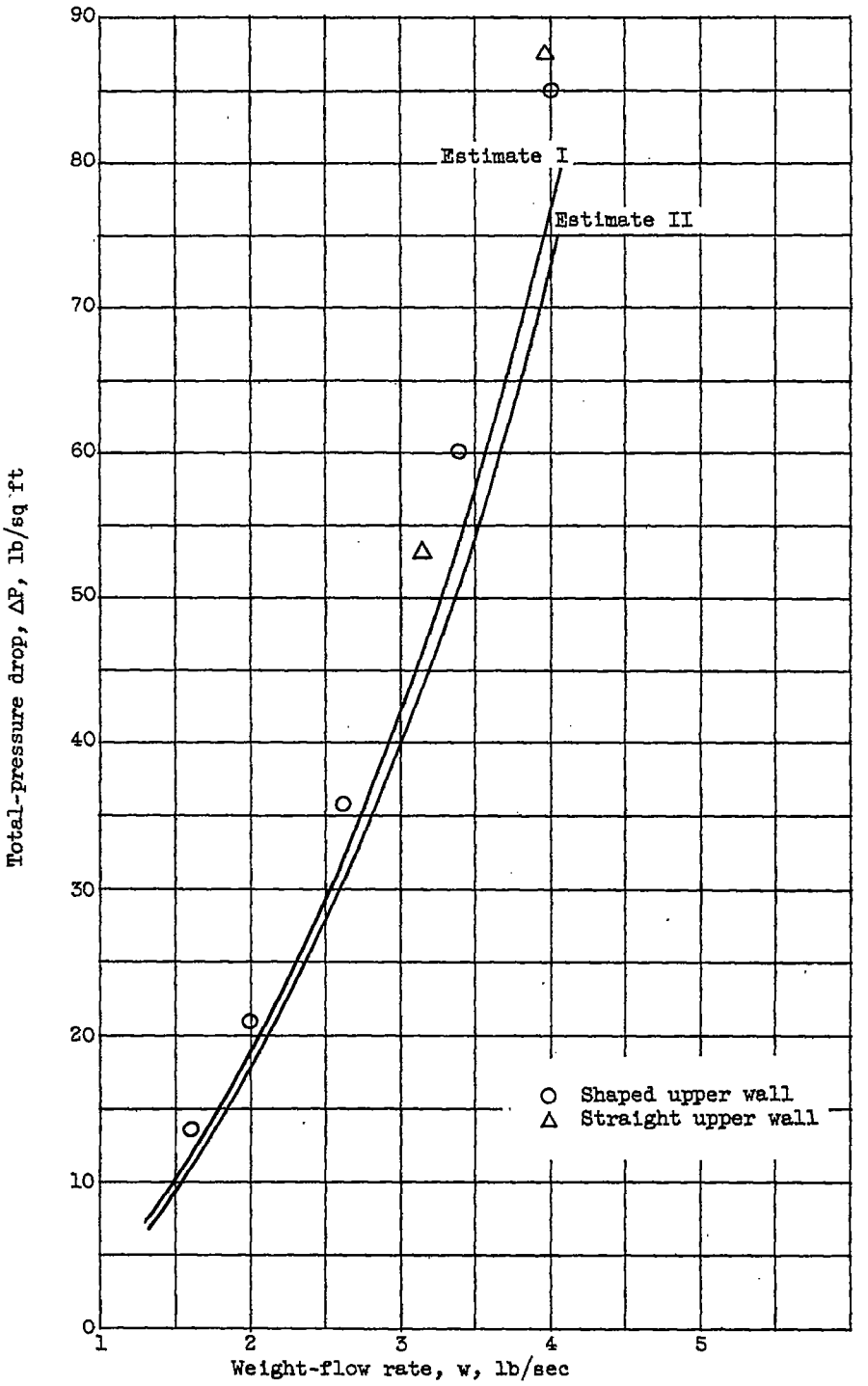

(a) Plate only.

Figure 10. - Variation of total-pressure drop with flow rate compared with estimated limiting curves of reference 7.

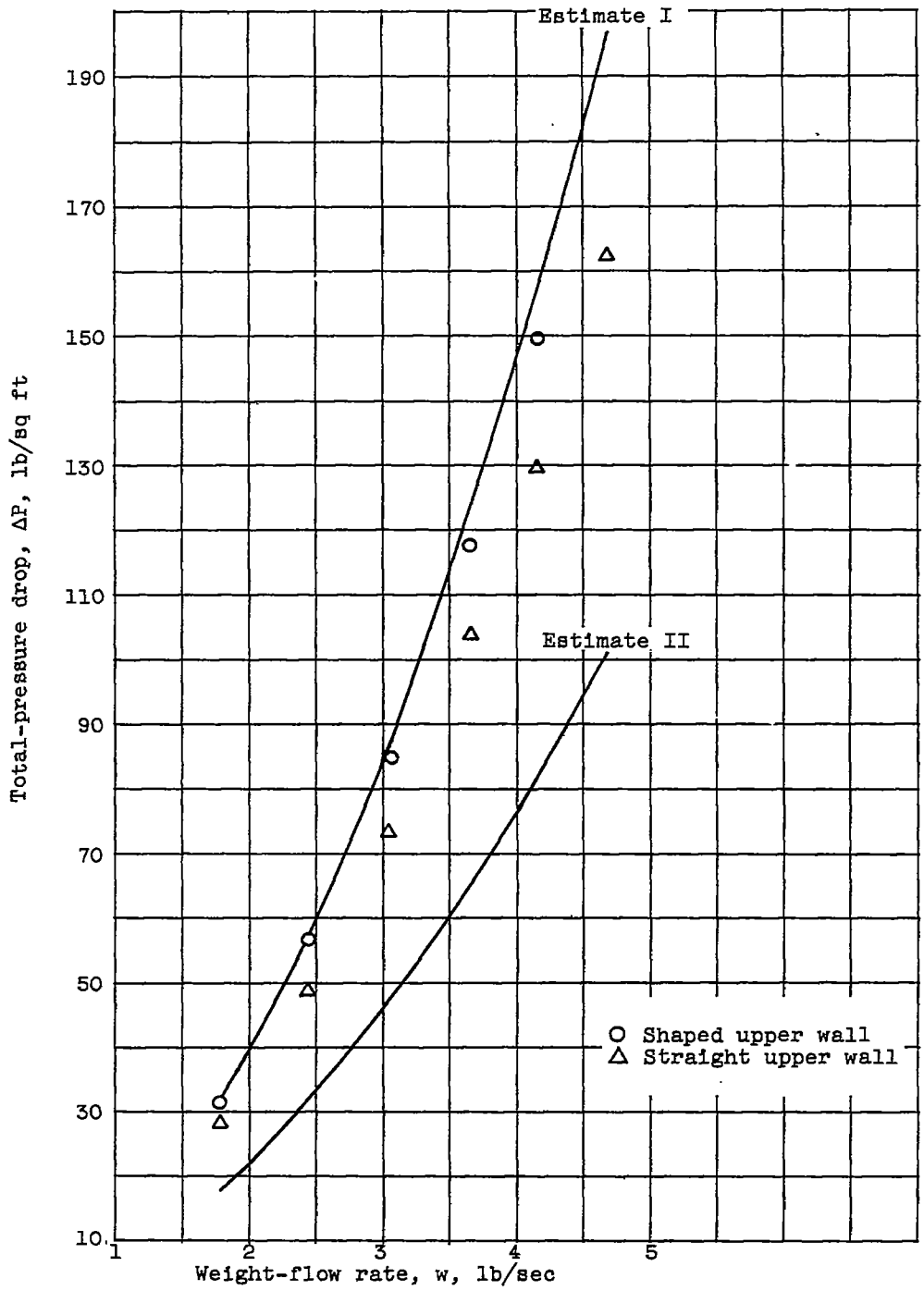

(b) Plate and one cloth.

Figure 10. - Continued. Variation of total-pressure drop with flow rate compared with estimated limiting curves of reference 7.

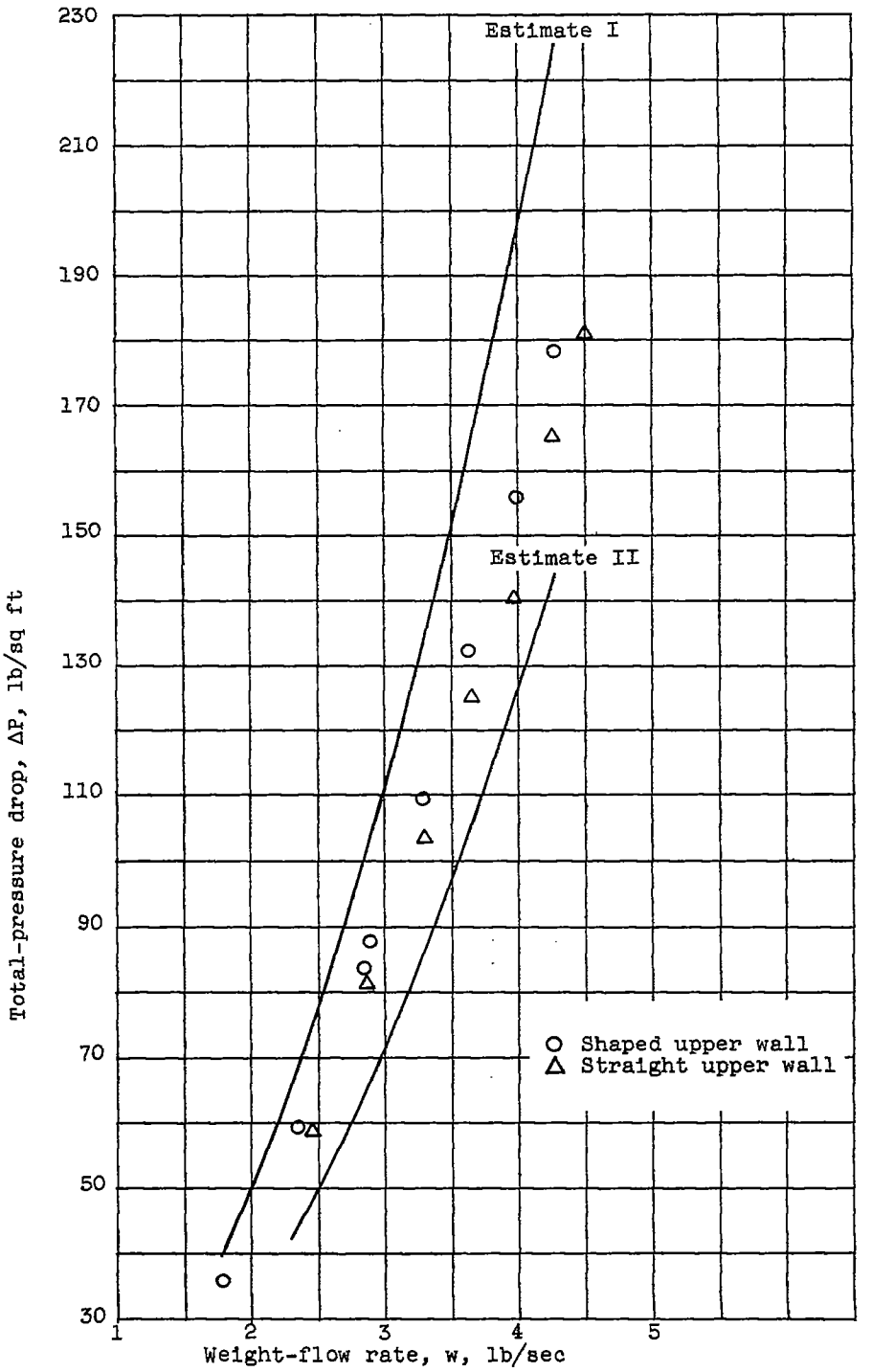

(c) Plate and two cloths.

Figure 10. - Concluded. Variation of total-pressure drop with flow rate compared with estimated limiting curves of reference 7.

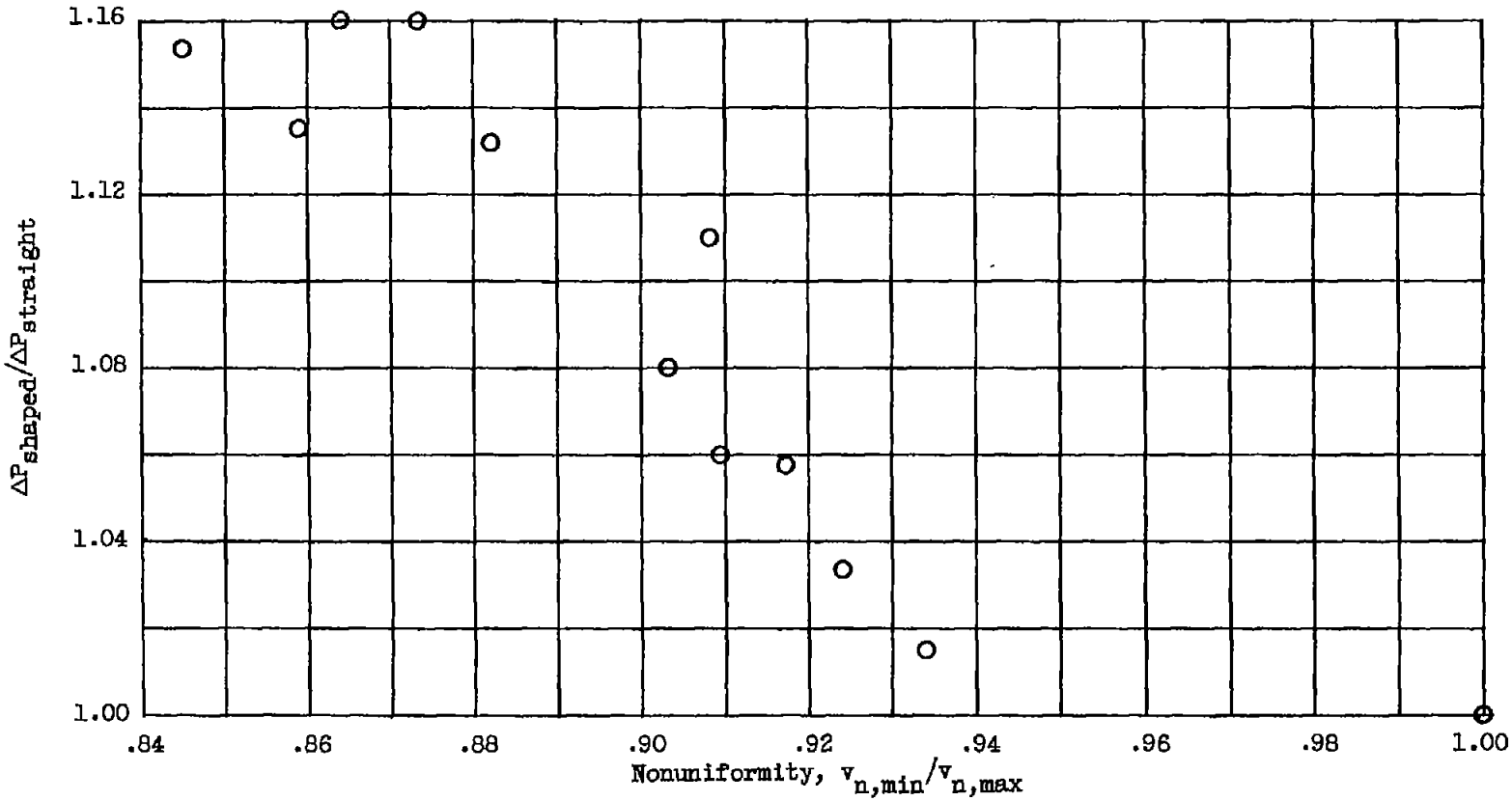

Figure 11. - Effect of nonuniformity of uncorrected flow on total-pressure loss after correction.

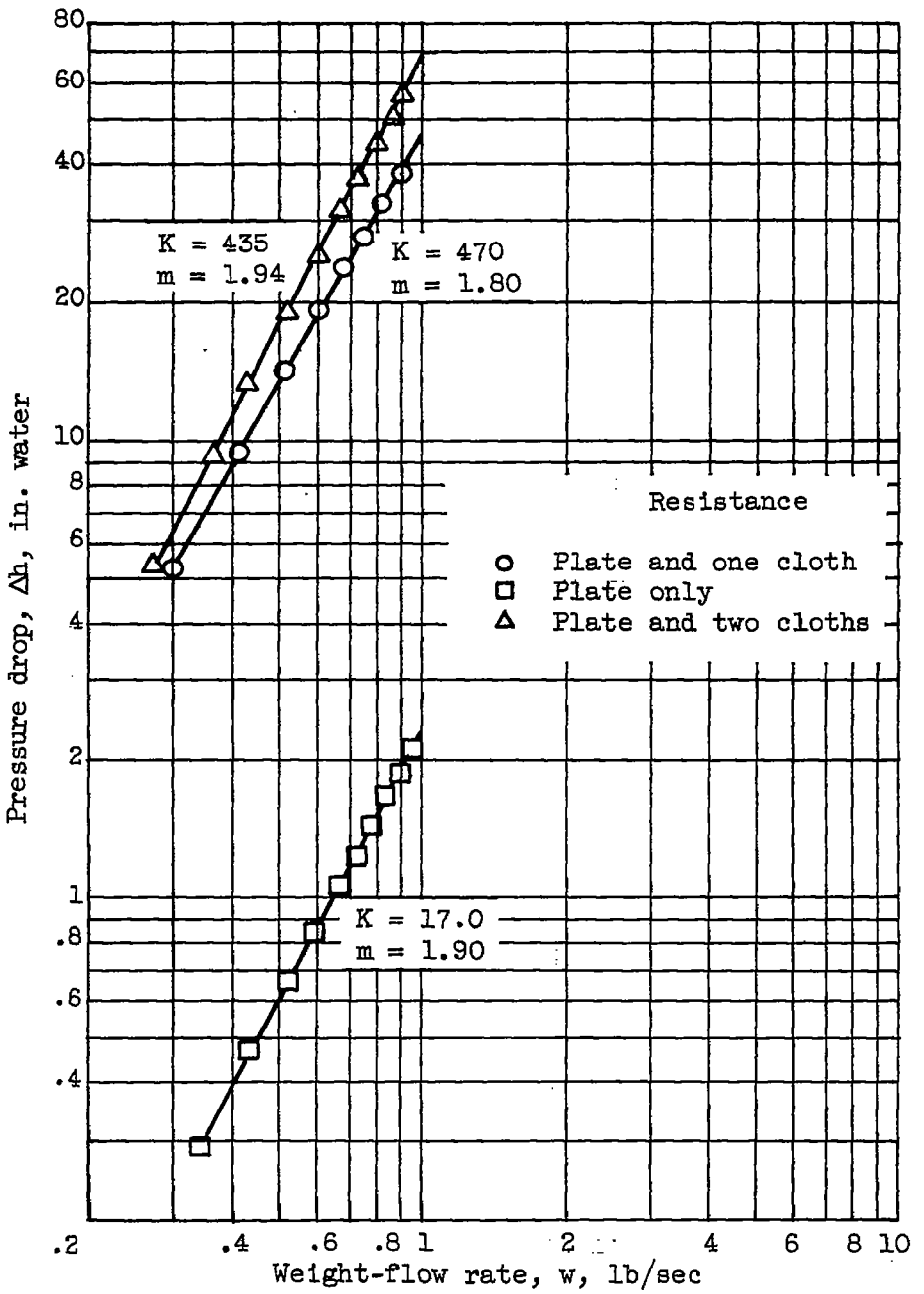

Figure 12. - Resistance curves for straight-through runs.